Spectrochimica Acta Part A: Molecular and Biomolecular Spectroscopy 260 (2021) 119919

Contents lists available at ScienceDirect

Spectrochimica Acta Part A: Molecular and Biomolecular Spectroscopy

journal homepage: www.elsevier.com/locate/saa

Bimolecular quenching of tryptophan fluorescence in a membrane protein: Evolution of local solvation and environment during folding into a bilayer

DeeAnn K. Asamoto [1], Ivan A. Kozachenko [1], Ignacio López-Peña, Judy E. Kim *

Department of Chemistry and Biochemistry, University of California, San Diego, La Jolla, CA, United States

HIGHLIGHTS

- Desolvation kinetics of the folding of a membrane protein, OmpA, were probed with Stern-Volmer experiments.
- Time-resolved Stern-Volmer analysis utilized sphere-of-action quenching model.
- Single tryptophan OmpA mutants provided site-specific changes in the kinetics of desolvation.
- Evolution of tryptophan environment and desolvation occur on different timescales.

GRAPHICAL ABSTRACT

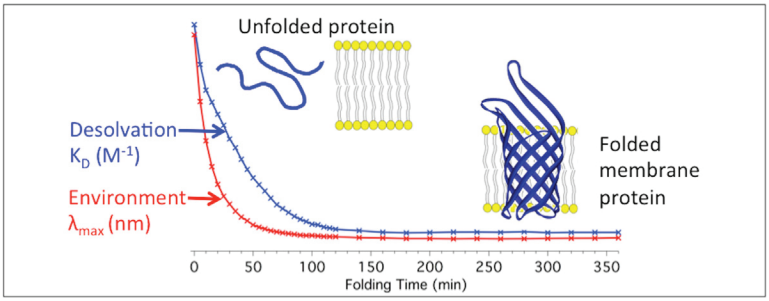

ARTICLE INFO

Article history:
Received 7 March 2021
Received in revised form 29 April 2021
Accepted 2 May 2021
Available online 5 May 2021

Keywords:
Membrane protein folding
Vesicles
Stern-Volmer
Desolvation
Kinetics

ABSTRACT

Fluorescence spectroscopy, including Stern-Volmer quenching, is a valuable tool for the study of protein dynamics. Changes in protein solvation during the folding reaction of a membrane protein, Outer membrane protein A (OmpA), into lipid bilayers was probed with bimolecular fluorescence quenching with acrylamide quencher. Six single-tryptophan OmpA mutants (W7, W15, W57, W102, W129, and W143) allowed for site-specific investigations at varying locations within the transmembrane β-barrel domain. A sphere-of-action quenching model that combines both static and dynamic components gave rise to Stern-Volmer quenching constants, K_D, for OmpA denatured in 8.0 M urea, aggregated in 0.5 M urea, adsorbed onto small unilamellar vesicles (SUVs), and folded in SUVs (t = 6 hrs). The average K_D values were $K_D^{denatured}(6.4\ M^{-1}) > K_D^{aggregated}\left(5.9\ M^{-1}\right) > K_D^{adsorbed}(1.9\ M^{-1}) > K_D^{folded}(0.6\ M^{-1})$. With knowledge of the fluorescence lifetimes in the absence of quencher, the bimolecular quenching constants, k_q, were derived; the evolution of k_q (and therefore K_D)during the folding reaction into SUVs (t = 0 hr to t = 6 hrs) revealed desolvation timescales, τ_{desolv} of 41–46 min (W7, W15, W57, W102), 27 min (W129), and 15 min (W143). The evolution of λ_{max} during folding revealed fast and slow components, $\tau_{environment}^{fast}$ and $\tau_{environment}^{slow}$ of 7–13 min and 25–84 min, respectively, for all mutants. For the five lipid- facing mutants (W7, W15, W57, W129, and W143), the general trend was $\tau_{environment}^{fast}(7-13\ min) < \tau_{desolv}(15-46\ min) \leq \tau_{environment}^{slow}(25-84\ min)$. These results suggest that there is an initial fast step in which there is a large change in polarity to a hydrophobic environment, followed by a slower desolvation process during evolution within the hydrophobic environment. These results complement previous mechanisms of concerted folding and provide insights into site-specific changes in solvation during formation of native β-barrel structure.

* Corresponding author.
E-mail address: judyk@ucsd.edu (J.E. Kim).
[1] D.K.A and I.A.K. contributed equally to this manuscript.

https://doi.org/10.1016/j.saa.2021.119919
1386-1425/

1. Introduction

1.1. The role of water during protein folding

A longstanding question in the study of membrane proteins is their folding mechanisms, and in particular, the process of transition from aqueous to lipid solvation during a folding process. The idea that water significantly influences the insertion and folding of membrane proteins is consistent with the extensive literature that elucidates the significance of water in the dynamics and structures of proteins and membranes. For example, water expulsion and inclusion are crucial for native structures [1], protein–protein recognition [2], and folding pathways [3].

There has also been effort to elucidate the dynamics of water at the interface and interior of lipid bilayers and proteins. The internal water molecules in folded proteins are exchangeable, as supported by studies of water penetration, mobility, and exchange in folded proteins [4–6]. NMR studies on proteins have revealed that surface-bound waters exchange rapidly (nanoseconds), while buried solvent molecules have longer residence times (up to milliseconds) [5,7]. These and other studies have aimed to elucidate the role of water in structure and folding of soluble proteins, but few experiments have probed the hydration status during a membrane protein folding reaction.

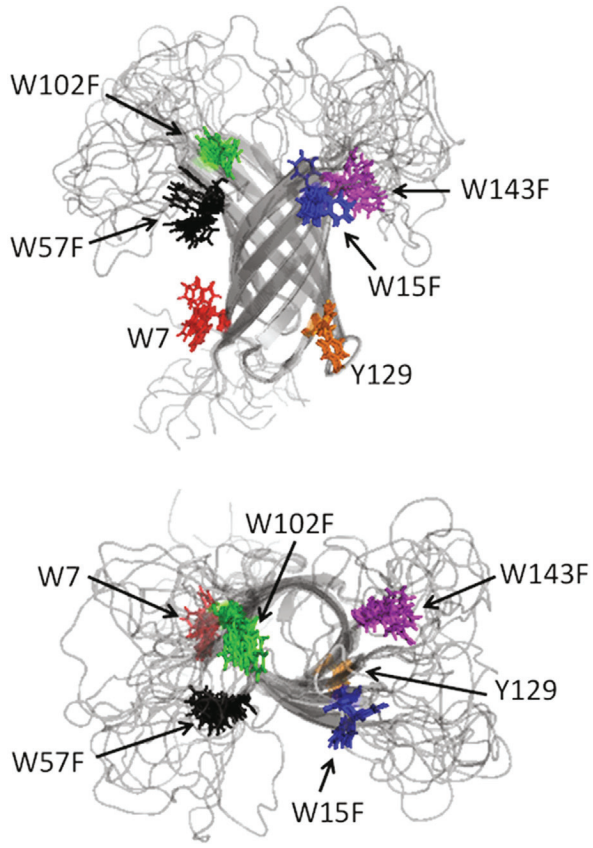

Fig. 1. OmpA structure. Solution NMR structures (10 conformers) of the transmembrane domain of OmpA mutant with single tryptophan at position 7 (PDB ID 2GE4). The dynamics of the native tryptophan at position 7 (W7) is shown in red. The remaining four native tryptophan residues at positions 15, 57, 102, and 143 were mutated to phenylalanine for the NMR study and are shown in blue (W15F), black (W57F), green (W102F), and pink (W143F), respectively. The native tyrosine residue at position 129 that was mutated to tryptophan for our present studies is highlighted in orange (Y129). The bottom structure shows a top down view of the transmembrane domain with a view looking down the center of the barrel.

1.2. Folding of outer membrane protein A

The inherent challenges associated with membrane proteins have restricted studies of membrane protein folding to a small subset of proteins amendable to *in vitro* experiments. Outer membrane protein A (OmpA) is one such system for studies of membrane protein folding. OmpA is an integral membrane protein that is found in the outer membrane of *E. coli* [8]. It forms an N-terminal, 8-stranded, transmembrane β-barrel and has a C-terminal soluble, periplasmic domain [9,10]. OmpA influences cell shape [11,12], is necessary for the action of colicin [13,14], and serves as a receptor for F-mediated conjugation and bacteriophage TulI [15,16].

OmpA is soluble in 8 M urea [17] and has been shown to spontaneously fold and insert into curved [18,19] lipid bilayers in an oriented fashion upon dilution of denaturant and in the absence of detergents [20]. The absence of the need for detergents is a benefit of OmpA in terms of protein folding studies. Another benefit of OmpA is the existence of high-resolution structural data. X-ray diffraction [21] and solution NMR [22] studies have provided atomic resolution structures of the OmpA transmembrane domain (Fig. 1). The breadth of previous of studies of OmpA makes it a very good system for the study of integral membrane protein folding.

OmpA has five native tryptophan residues located near the membrane-aqueous interface at positions 7, 15, 57, 102 and 143 (Fig. 1). The tryptophan residue at position 7 is located on the periplasmic region of the outer membrane, while tryptophan residues 15, 57, 102 and 143 are on the extracellular side of the outer membrane. Tryptophan fluorescence during OmpA folding has been well characterized in micelles [23], small unilamellar vesicles (SUVs) [20], amphipols [24], and nanodiscs [25]. Tryptophan fluorescence has also been used to study the kinetics of the OmpA folding reaction into lipid bilayers via investigation of single tryptophan OmpA mutants; these data support a model of concerted folding [26]. Förster resonance energy transfer (FRET) studies have determined distances between the native tryptophan residues using cysteine linked dye molecules in different unfolding states of OmpA [27].

1.3. Bimolecular quenching and solvent accessibility

Measurements of bimolecular fluorescence quenching with external quenchers report on the solvent accessibility of native tryptophan residues and may provide additional details about its folding mechanism into lipid bilayers [28]. Tryptophan fluorescence is efficiently quenched by acrylamide through a combination of collisional (dynamic) and static mechanisms [29,30]. The analysis involves generation of a Stern-Volmer plot. In collisional quenching, the quencher diffuses to the fluorophore within the lifetime of the excited state, makes *van der Waals* contact (<5 Å) [31], and deactivates the fluorophore to the ground state without the emission of a photon. Fluorescence quenching may also reflect contributions from a static process in which the fluorophore and quencher form a non-fluorescent, ground-state complex. The presence of static quenching has been observed in single-tryptophan containing proteins in the presence of acrylamide [32]. It is believed that indole and acrylamide have a relatively weak association within a "sphere-of- action" volume where the fluorescence is immediately quenched within this volume. These bimolecular quenching mechanisms differ from those that rely on longer-range dipole–dipole mechanisms, such as FRET, and thus report on more local photophysical effects.

If tryptophan is solvent-exposed and accessible to a quencher, such as acrylamide, the fluorescence is quenched, leading to decreased fluorescence intensity. If tryptophan is buried and inaccessible to solvent, acrylamide may not diffuse to tryptophan within the lifetime of the excited state to quench the fluorescence.

If tryptophan is partially exposed to solvent, the extent of quenching is moderate. In this manner, the extent of quenching reflects changes in quencher accessibility; for a water-soluble quencher, bimolecular quenching data can be interpreted to reflect evolution of solvent accessibility of tryptophan during membrane protein folding.

1.4. Changes in local environment during OmpA folding

The requirement of *van der Waals* contact for both static and dynamic quenching, and the decreased amount of water [6] (and soluble quenchers) in lipid bilayers allows these experiments to provide information on accessibility of quencher to fluorophore during folding. Time-resolved distance determination by fluorescence quenching experiments using brominated lipids were previously performed to track the distance between tryptophan residues and the center of the lipid bilayer during the folding of OmpA [26,33,34]. Other steady-state quenching studies with OmpA and soluble quenchers have focused on folded and unfolded states, but to the best of our knowledge, there have been no time-resolved experiments to monitor the change in solvent accessibility of single-tryptophan residues during the folding reaction of OmpA.

This report describes changes in solvent accessibility for tryptophan during the folding and insertion of OmpA into SUVs. The temporal evolution of the Stern-Volmer plot during the folding reaction provides insight into the kinetics of transfer from bulk aqueous to bulk lipid environment, a process we refer to as desolvation. These results complement analogous changes in the emission maxima during folding and lead to new insights into the folding reaction.

2. Materials and methods

2.1. Sample preparation

Chemicals used in the experiments include N-acetyltryptophanamide (Sigma Aldrich), ultra pure urea (MP Biomedicals), acrylamide (Thermo Fisher Scientific), dipotassium phosphate (Thermo Fisher Scientific), and potassium dihydrogen phosphate (Thermo Fisher Scientific). These reagents were used as received.

OmpA mutants that contain single tryptophan residues were expressed and purified following an established procedure [10]. These mutants, referred to as single-tryptophan mutants, were prepared with single tryptophan residues at native (7, 15, 57, 102, 143) or non-native (Y129W) positions. In these mutants, the remaining four or five (in the case of 129) native tryptophan residues were mutated to phenylalanine. These OmpA mutants are referred to as W7, W15, W57, W102, W143, and W129. An additional mutant, in which all tryptophan residues were replaced with phenylalanine was also generated; this mutant is called W0. The protein was overexpressed in an OmpA-free stock JF733 and the cells were lysed by sonication after treatment with lysozyme. The membranes were collected by centrifugation, and OmpA was extracted with a solution of urea and isopropanol. The crude protein was purified on a Q sepharose Fast Flow (GE Healthcare Life Sciences) anion exchange column and eluted by a NaCl gradient. The protein-enriched fractions were combined and concentrated by ultrafiltration (Millipore Ultracel NMWL 3 or 10 KDa). The samples were stored in the denatured state (8.0 M urea, 20 mM potassium phosphate buffer, pH 7.3), with stock concentrations of 150–400 μM. All protein samples described in this report contained 20 mM potassium phosphate buffer, pH 7.3, referred to as KPi buffer.

2.2. Preparation of samples for fluorescence experiments

SUVs of dimyristoylphosphatidylcholine (DMPC, phase transition temperature T_m = 24 °C) and dipalmitoylphosphatidylcholine (DPPC, T_m = 41 °C) were prepared according to a previously published procedure [10]. The lipids were purchased from Avanti Polar Lipids. Briefly, 25 mg of lipid dissolved in chloroform was dried under nitrogen gas for several hours. The dry lipid film was resuspended in 5 mL of KPi buffer with a bath sonicator and SUVs were formed using a probe sonicator tip. The SUVs were filtered through a 0.22 μm pore polyvinylidene fluoride filter, resulting in a 5 mg/mL (7.375 mM) lipid stock solution. The SUVs were allowed to equilibrate overnight above their phase transition temperature prior to experiments. The diameter of the vesicles was approximately 50 nm based on dynamic light scattering (DLS) experiments. DMPC SUVs were used for the study of the folding and insertion of OmpA at 37 °C; DPPC SUVs were used to study the adsorbed state of OmpA at room temperature (~21 °C).

For each quenching experiment, five 200 μL samples were prepared with acrylamide concentrations of 0.0, 0.1, 0.2, 0.3, and 0.4 M; acrylamide was dispensed from a 1.0 M stock solution. Protein was added to solutions that contained SUVs and acrylamide (if appropriate) in KPi. Denatured OmpA was obtained from a secondary stock solution that contained 80–140 μM OmpA and 5.0 M urea. OmpA has been reported to be denatured in 4.0 M urea [20]. The final protein concentration varied between 8 and 14 μM based on the absorption spectra of protein in the 0.0 M acrylamide sample. The final urea concentration was 0.5 M for all samples because each sample was comprised of a 10-fold dilution of the secondary stock. The final lipid concentration was 2 mg/mL (2.950 mM), which gave a lipid to protein ratio of 300:1 for the targeted 10 μM protein and resulted in folding yields of 78–100% across all mutants. All samples were mixed thoroughly after injecting 20 μL of the protein secondary stock into 180 μL of the temperature-equilibrated SUV and acrylamide solution. This mixing was performed immediately, within 10 s, before the first fluorescence spectrum was acquired. Each cuvette was covered with a parafilm-sealed Teflon cap.

2.3. Spectroscopic measurements of fluorescence quenching

Fluorescence spectra were acquired on a Jobin Yvon Fluorolog Spectrofluorometer FL3-11. The emission window was 300 nm to 500 nm, and spectra were acquired with 4-nm step size with 0.5-second integration time and 3-nm entrance and exit bandpass; the excitation wavelength was 290 nm. The fluorescence spectra were collected as one accumulation. Temperature was maintained at 37 °C for the OmpA folding study, and at room temperature (~21 °C) for the adsorbed (DPPC), unfolded (8.0 M urea) and aggregated (0.5 M urea) OmpA experiments. The temperature-dependence of tryptophan emission was investigated. The wavelength of maximum emission remained 360 nm and the fluorescence intensities decreased ~23% with an increase in temperature from 21 °C to 37 °C (data not shown).

For the folding experiment, acquisition of fluorescence spectra commenced upon addition of 20 μL of the secondary OmpA stock into five 2 × 10 mm quartz cuvettes, each of which contained 180 μL of a pre-made, temperature equilibrated, solution of KPi, DMPC SUVs, and varying concentrations of acrylamide. The final samples (200 μL total volume) were excited with 290 nm light along the 2 mm path and fluorescence was acquired along the 10 mm path. During a folding experiment, spectra were acquired for each sample at 5-minute intervals for the first two hours, and then at 20-minute intervals for the remaining 4 h of the experiment (6 h total). The fluorescence spectra of protein with five acrylamide concentrations (0.0, 0.1, 0.2, 0.3 and 0.4 M) were acquired

in parallel, on the same day. To optimize the signal and collect spectra efficiently, sufficiently high protein concentration and relatively large step size (4 nm/step) were utilized. Fluorescence spectra of blanks that contained vesicles, acrylamide (if appropriate), and KPi were also acquired at the beginning and end of each experiment. Absorption spectra of each sample were acquired on an Agilent 8453 UV–visible spectrophotometer along the 10 mm path length of the cuvette after the experiments were completed.

Analogous experiments were conducted for one hour at room temperature with DPPC SUVs to investigate the kinetics of the adsorption process of OmpA. Spectra were collected every 5 min for the first 30 min and then every 10 min for the remaining 30 min (1 h total). Aside from the decreased duration of the experiment, lower temperature, and gel phase vesicles, all aspects of the adsorbed experiment and data workup procedure were identical to the 6-hour folding experiment with DMPC SUVs.

Other experiments were conducted at room temperature for unfolded (8.0 M urea) and aggregated (0.5 M urea) OmpA in the absence of SUVs; these experiments revealed the level of quenching for the fully denatured and aggregated states of OmpA. For these experiments, samples were incubated for 5 min at room temperature, followed by collection of fluorescence spectra with 1-nm step size and 1-second integration time. All other fluorescence parameters as well as protein and acrylamide concentrations were the same as the previously described folding experiments.

2.4. Vesicle leakage assays

Vesicle leakage assays were conducted to investigate the stability and permeability of the SUVs. Prior to sonication, the aqueous DMPC solution contained 50 mM 8-aminonaphthalene-1,3,6-trisulfonate (ANTS), a fluorophore, 50 mM *p*-xylene-bis(N-pyridinium bromide) (DPX), a FRET quencher for ANTS [35,36], and 2.5 mg/ml resuspended DMPC. The reagents ANTS and DPX were purchased from Thermo Fisher and stored in a desiccator, in the dark, prior to use. The decrease in lipid stock concentration to 2.5 mg/ml relative to folding experiments (5 mg/ml) was necessary to avoid flocculation of the lipid + dye solutions. After sonication, 3.0 mL of the 2.5 mg/ml DMPC SUV stock solution with ANTS and DPX was passed down a warm (~45 °C) 10DG desalting column (Bio-Rad Laboratories) to separate vesicles encapsulating ANTS + DPX from free ANTS and free DPX by size exclusion. After discarding the initial dead volume of 3.0 mL, 0.5 mL fractions were collected. The first 3.5 mL of elution were tested for encapsulation of ANTS + DPX by acquisition of fluorescence spectra before and after lysis of the SUVs in the presence of 0.1% (v/v) [37] Triton X-100 detergent; this concentration of Triton X-100 was obtained by 10x dilution of an initial 1% Triton X-100 solution purchased from MP Biomedicals. ANTS fluorescence spectra were collected from 400 nm to 670 nm with 1-nm step size, 1-second integration time, and 3-nm entrance and exit bandpass; the excitation wavelength was 380 nm [38]. Increase in fluorescence intensity after lysis indicated that the first 1.0 mL of elution was the most enriched in SUVs encapsulating ANTS + DPX.

The effects of acrylamide and OmpA on the integrity of the SUVs were investigated. In one experiment, two 180 μL samples of ANTS + DPX-encapsulated DMPC SUVs from the first 1.0 mL of elution were prepared with and without 0.4 M acrylamide and then incubated at 37 °C. Fluorescence and absorption spectra were monitored over a period of 6 h. In a separate experiment, a sample of the ANTS + DPX-encapsulated SUVs was prepared with ~10 μM OmpA in a manner analogous to the folding experiment. The fluorescence of tryptophan (excitation at 290 nm and emission from 300 to 500 nm) and ANTS (excitation at 380 nm and emission from 400 to 670 nm) were monitored over time. For both experiments, fluorescence spectra were acquired over 6 h, at 20-minute intervals for the first 3 h and then at 30-minute intervals for the last 3 h. The samples were then lysed by adding 20 μL of 1% Triton X-100 to create a 0.1% Triton X-100 solution, and fluorescence and absorption spectra were measured on this lysed sample.

2.5. Dynamic light scattering experiments

DLS experiments were conducted to evaluate the diameter of the SUVs and to investigate potential effects of acrylamide on their size and stability. Samples of 2 mg/ml DMPC were prepared in the presence of 0.0, 0.2 and 0.4 M acrylamide, and maintained at 37 °C. DLS data were acquired at 3-hour intervals. The 1.01 Watt 532 nm output from a diode-pumped Nd:YVO_4 laser (Coherent Verdi) was attenuated with neutral density filters to ~50 mW, focused with a 100 mm focal length lens and directed vertically through the sample in a 10 × 10 mm quartz cuvette. Scattered light that passed through a small aperture (<1 mm diameter) was collected at 90° relative to the incident beam by a SPEX double monochromator. Photons were detected by an Amprex Model 56 photomultiplier tube, and the output was amplified and discriminated (Tennelec 454) to produce standard pulses suitable for counting; the signal was accumulated in a multichannel scaler (ComTec GmbH FAST multichannel analyzer). Each acquisition was comprised of 20 μs bins for a total accumulation time of 10.5 s; for each sample, 20 acquisitions were acquired. The fluctuation in the intensity of the scattered signal revealed the radii of the SUVs [39].

2.6. Fluorescence quenching data analysis

The raw fluorescence spectrum is comprised of fluorescence from OmpA as well as scattering from SUVs. The fluorescence originates from the single tryptophan and 16 or 17 native tyrosine residues in OmpA; subtraction of the signal from tyrosine did not significantly affect the quenching or decay constants (see below and Supporting Information). Therefore, all spectra were treated in the following manner, without subtraction of tyrosine signal. OmpA fluorescence spectra were isolated by subtracting a scalar multiple of the blank spectrum from each raw spectrum to generate a difference spectrum: OmpA fluorescence spectrum = (raw OmpA spectrum) − (c × blank spectrum), where c is a scalar between the values of 0.5 and 1.5 and the blank spectrum exhibits signal from all components of the solution except protein. The selection of c was based on the known spectral profile of OmpA emission for high concentration sample where scattering is less prominent; the difference spectrum properly reproduced the blue-shifted fluorescence and increase in fluorescence quantum yield during folding. Emphasis was placed on the region near 300 nm, where the scattering signal is greatest, and values of c were selected to avoid over- or under-subtraction, especially in this region (see Supporting Information). These difference spectra that contained signal from OmpA only are referred to as isolated OmpA fluorescence spectra.

The isolated OmpA fluorescence spectra, called F_{obs}, were further corrected for the inner-filter effect, which is attenuation of the excitation beam and emission signal by the sample itself. This correction yielded a new corrected OmpA fluorescence spectrum referred to as F_{corr} [28]. The equation for the inner-filter effect is given:

$$F_{corr} = F_{obs} 10^{\left(\frac{A_{ex}+A_{em}}{2}\right)} \quad (1)$$

In Eq. (1), A_{ex} and A_{em} are the absorbance at the excitation and emission wavelengths, respectively (A_{ex} is 290 nm). The maximum absorbance at 290 nm across all mutants and all trials, prior to the correction for the inner filter effect, was 0.69. This absorbance value includes contribution from vesicles, protein, and 0.4 M acry-

lamide. Despite the blue-shift of the fluorescence maximum from ~350 nm to ~330 nm, the wavelength used for A_{em} was kept constant at 350 nm. The difference in absorption for 350 nm and 330 nm is negligible in terms of the inner-filter effect correction for tryptophan. In similar studies on OmpA, A_{em} was disregarded because of negligible absorption at the emission wavelengths [33]. To determine A_{ex} and A_{em}, absorption values along the 2 mm pathlength for the relevant wavelengths were determined. The assumption of 2 mm pathlength for both excitation and emission paths is an estimate because the pathlength of the emitted light is probably close to 5 mm, which is half the total pathlength of 10 mm. However, given the negligible effect of A_{em} (value of A_{em} at 350 nm was typically 0.003 over 1-cm pathlength), the use of 2 mm vs 5 mm pathlength for emission does not significantly affect the self-absorption correction. Gaussian fits were applied to the peaks of all corrected fluorescence spectra to determine maximum fluorescence intensities (F_{max}) and maximum fluorescence wavelengths (λ_{max}).

OmpA concentrations for samples that contained acrylamide could not be determined from absorption spectra because the absorbance of acrylamide overlapped with the 280-nm protein band. Thus, it was especially important that sample preparation and initiation of the folding reaction were carefully and reproducibly executed. It was assumed that the concentrations of protein in the 0.1, 0.2, 0.3, and 0.4 M acrylamide samples were identical to that in 0.0 M acrylamide; the latter was determined by UV–Vis absorption measurements. Reported errors in the experiments reflect, in part, variation in protein concentration.

Stern-Volmer plots were constructed from values of F_{max} for all five samples with different acrylamide concentrations at each time point during the folding reaction. Briefly, the corrected fluorescence intensity of each sample (0.1–0.4 M acrylamide) (F_{max} abbreviated simply as F) was compared to the corrected fluorescence intensity in the absence of quencher (0.0 M acrylamide) (F_0) by the ratio $\frac{F_0}{F}$ and plotted versus [acrylamide]. The intensities were determined at the wavelength corresponding to maximum emission intensity. For the 6- or 1- hour DMPC (folding) and DPPC (adsorbed) experiments, respectively, Stern-Volmer plots were constructed for each time point. The plots were fit to the standard, linear dynamic quenching model to yield K_{SV} values as well as a combined dynamic-static quenching model to yield K_D values. The latter model utilized the sphere-of-action equation, which has been associated with the tryptophan-acrylamide system [28].

$$\text{Dynamic model}: \quad \frac{F_0}{F} = K_{SV}[Q] + y_{int} = k_q\tau_0[Q] + y_{int} \tag{2}$$

$$\text{Sphere}-\text{of}-\text{action model}: \quad \frac{F_0}{F} = (K_D[Q] + y_{int})e^{V[Q]} = (k_q\tau_0[Q] + y_{int})e^{V[Q]} \tag{3}$$

In Eqs. (2) and (3), F_0 represents the fluorescence intensity of the fluorophore (tryptophan) in the absence of quencher, while F indicates the maximum, corrected fluorescence intensity in the presence of quencher. Under ideal experimental conditions, the value of the y-intercept (y_{int}) should be 1. In the present analysis, y_{int} was allowed to vary between 0.95 and 1.05 to take into account slight experimental offsets. The quencher concentration, [Q], is that of acrylamide. In the dynamic model (Eq. (2)), the Stern-Volmer quenching constant reflects purely dynamic (collisional) quenching and is denoted K_{SV}. In the sphere-of-action model, there is a dynamic quenching component, denoted K_D, as well as a static volume (V), called the "sphere of action", within which the probability of quenching is unity. In the present experiments, values of V were determined for the different conformations of denatured, adsorbed, and aggregated OmpA. Additionally, the values of V at the t = 0 and t = 6 hr timepoints during folding were determined for each mutant. An average value of V based on the combined t = 0 and t = 6 h timepoints for all mutants was also determined. The dynamic constants K_{SV} and K_D are the product of the bimolecular quenching constant (k_q) and lifetime of the fluorophore in the absence of quencher (τ_0). The published values of τ_0 for OmpA were utilized [40], and the values of k_q derived from K_D were plotted as a function of folding time. These kinetic traces were averaged for multiple trials and fit to single or double exponential decay functions.

2.7. SUV leakage data analysis

The optimal sample of SUVs that encapsulated ANTS and DPX and that eluted from the column was selected by comparing the increase in fluorescence signal upon 100% lysis with Triton-X. The fluorescence spectrum of the fraction that revealed the largest change in signal upon lysis was subtracted of their water Raman signal. The fluorescence spectra were not normalized for concentration of fluorophore because the leakage caused by protein or acrylamide was assessed relative to 100% lysis on the same sample. This relative leakage was visualized in plots of fluorescence maxima (514 nm) before and after addition of OmpA or acrylamide (as a function of time), compared to the spectrum for lysis with Triton X.

3. Results

The change in solvent accessibility during the folding and insertion of OmpA into SUVs was studied via bimolecular fluorescence quenching. For a given OmpA mutant, five samples of 8–14 μM protein were prepared with DMPC SUVs and increasing concentrations of acrylamide (0.0, 0.1, 0.2, 0.3 and 0.4 M). Each experiment resulted in the collection of 185 spectra (37 spectra for each of five acrylamide concentrations corresponding to 37 time points over 6 h). SDS-PAGE differential mobility analysis was performed to confirm that the presence of acrylamide did not significantly hinder the folding yield; the yield changed less than 10% in 0.4 M acrylamide relative to in the absence of acrylamide. Representative fluorescence data for each mutant is shown in Supporting Information. Representative data for the folding of W102 into SUVs in the absence of acrylamide and presence of 0.4 M acrylamide are shown in Fig. 2. These spectra show the characteristic blue-shift from ~350 nm to ~330 nm as well as increase in fluorescence quantum yield during folding into SUVs. The spectra indicate that the presence of acrylamide affects the wavelength of fluorescence in a subtle manner, but the relative blue-shift during folding is approximately the same for all acrylamide concentrations for a given mutant. The maximum tryptophan fluorescence intensities for all five acrylamide concentrations are plotted as a function of folding time in the Fig. 2 inset; these intensities were determined irrespective of the wavelength of emission, which varied systematically from ~350–327 nm for all mutants during the folding reaction.

Stern-Volmer plots were generated for each of the 37 time points during the folding reaction; Fig. 3 shows representative data for the Stern-Volmer plots of W102. The Stern-Volmer plots can be fit to the dynamic (Eq. (2)) or sphere-of-action (Eq. (3)) models. For the latter, proteins exhibit different values of V that depend on their conformation and effort was made to determine the most reasonable value of V.

It is expected that V should evolve during a folding reaction and this evolution leads to complexities in the analysis. A simple model was first tried: values of V = 0.0, 0.3, 0.6, and 0.9 M^{-1} were selected based on literature and utilized for all folding time points of all mutants. The resulting values of K_D for each of these four values

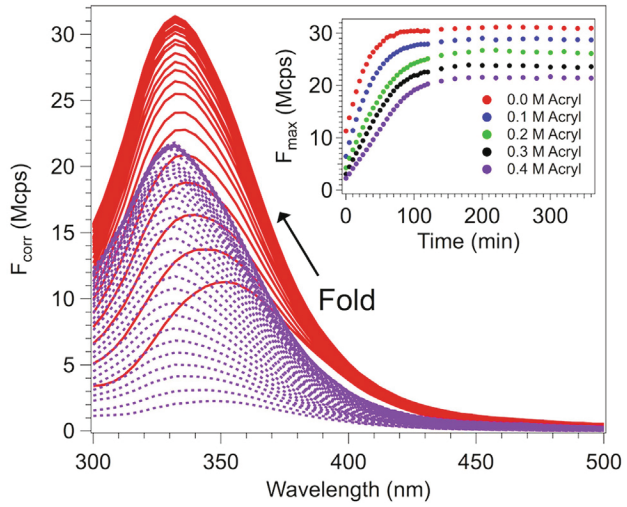

Fig. 2. Representative fluorescence data during the folding reaction in the absence and presence of acrylamide. Fluorescence spectra are shown for OmpA W102 in the absence (solid red curves) and presence of quencher (0.4 M acrylamide, dashed purple curves) during the folding reaction (0 to 6 h) into SUVs. The spectra are corrected for scattering from SUVs and signal from buffer as described in the main text and Supporting Information. The isolated OmpA spectra were further corrected for the inner filter effect using Eq. (1). Inset shows the maximum fluorescence intensity for each acrylamide concentration (0.0, 0.1, 0.2, 0.3, and 0.4 M) during the folding reaction.

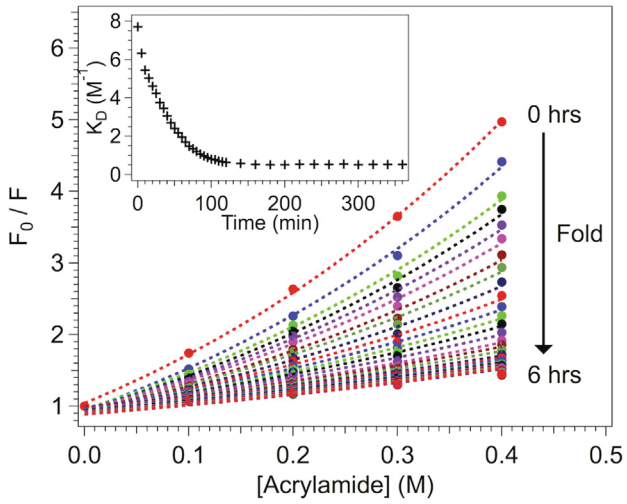

Fig. 3. Representative Stern-Volmer plots during the folding reaction. Stern-Volmer plots are for OmpA mutant W102 during the folding reaction (0–6 h) into SUVs. The dashed curves are fits to the data using the sphere-of-action model (Eq. (3)) with V held constant at 0.46 M^{-1}. The inset shows the evolution of K_D during the folding reaction.

of V were determined. The decays of K_D during folding were fit to an exponential function and the decay constant for each value of V was determined (Supporting Information); for all mutants except W7, the four values of the decay constants were within 5% of one another. For example, for W15 (n = 4), the reciprocal decay constant was 46, 46, 45, and 45 min for values of V = 0.9, 0.6, 0.3, and 0.0 M^{-1}, respectively. The average value for W15 for these four values of V was 45.5 min. W7 exhibited the greatest deviation of values of the decay constant, but still within 13% of one another: the reciprocal decay constant was 41, 45, 46, and 46 min for V = 0.9, 0.6, 0.3, and 0.0 M^{-1}, respectively (with average value of 44 min). The average value of the reciprocal decay constants were 44, 46, 43, 41, 28, and 15 min for the four values of V for W7, W15, W57, W102, W129, and W143, respectively.

As a more informed model, an average value of V of 0.46 M^{-1} was utilized for all time points and mutants during the folding reaction. This value of V was determined by performing a simultaneous fitting scheme, which we refer to as a global fit, across all trials of all mutants at the extremes where the value of V is expected to be largest (t = 0 hr) and smallest (t = 6 hr). For both of these time points, there were a total of 19 trials, with three trials each for W7, W57, W102, W129, and W143 and four trials for W15. The resulting value for V from this global fit were $V = 0.69\ M^{-1}$ for t = 0 hr (n = 19) and $V = 0.23\ M^{-1}$ for t = 6 hr (n = 19) time points (see Supporting Information). The average of these values is $V = 0.46\ M^{-1}$ (n = 38), and this value of V = 0.46 M^{-1} was used as the sphere-of-action volume for our analysis of the folding reaction of OmpA. Fig. 3 shows representative fits to the sphere-of-action model with V = 0.46 M^{-1} for W102 during folding; the corresponding decay of K_D during folding is shown as the inset. The average K_D decay curves for each mutant across all trials are shown in Supporting Information. The values of K_D were converted to k_q by taking into account τ_0, and k_q values were plotted as a function of folding time (Fig. 4 and Table 1). The conversion of K_D to k_q involves division of K_D with the lifetime (τ_0), so the exponential time constant is identical for K_D and k_q. The results from single exponential fits to the k_q decays gave rise to reciprocal time constants of 46, 46, 43, 41, 27, and 15 min for W7, W15, W57, W102, W129, and W143, respectively (Table 1). Single exponential fits to K_D with residuals are shown in Supporting Information. As a final analysis, K_{SV} and K_D values were compared and as expected, the values for K_{SV} are higher than K_D values (Table 1). Despite the superior fit of the data to the sphere-of-action model, however, the temporal evolution of K_{SV} and K_D were identical (Supporting Information).

OmpA in the denatured, aggregated, and adsorbed states were also investigated. Representative fluorescence spectra and Stern-Volmer plots are shown in Supporting Information. The values of V for denatured (8.0 M urea), aggregated (0.5 M urea), and adsorbed (DPPC SUVs) OmpA were determined using the same method as for the folding reaction. Namely, global fits to all mutants for each condition led to values of V of 0.80, 0.71, and 0.39 M^{-1} for denatured, aggregated, and adsorbed OmpA, respectively (Supporting Information). Corresponding values of K_D are provided in Table 1 and Supporting Information

The contribution of the tyrosine on Stern-Volmer quenching constants was determined by subtracting the spectrum of W0 from that of the tryptophan-containing mutant at a given time in the folding reaction. The tyrosine-free spectra were then analyzed in the same manner described above; representative data for W102 are shown in Supporting Information. The effect of tyrosine emission on the evolution of K_D during the folding reaction was minor, so the subtraction of W0 from each mutant was not needed.

The fluorescence wavelength at the maximum emission intensity, λ_{max}, was determined via Gaussian fits to the fluorescence spectra in the range 301 to 370 nm. This range was selected because it encompasses the emission maximum for all data sets and across all mutants. Data from multiple trials were averaged (Supporting Information), and the average wavelengths were plotted as a function of folding time. The characteristic blue-shift of the fluorescence wavelength during folding, from time 0 to 6 h, are shown in Fig. 4 (bottom panel) for all OmpA mutants. The presence of acrylamide did not significantly affect these observed changes in fluorescence wavelength during folding despite the fact that acrylamide led to a slight blue-shift of approximately 2 nm of the absolute fluorescence wavelengths (see Supporting Information). The modest blue-shift in the fluorescence wavelength in the presence of acrylamide was not observed for NATA. For all OmpA mutants,

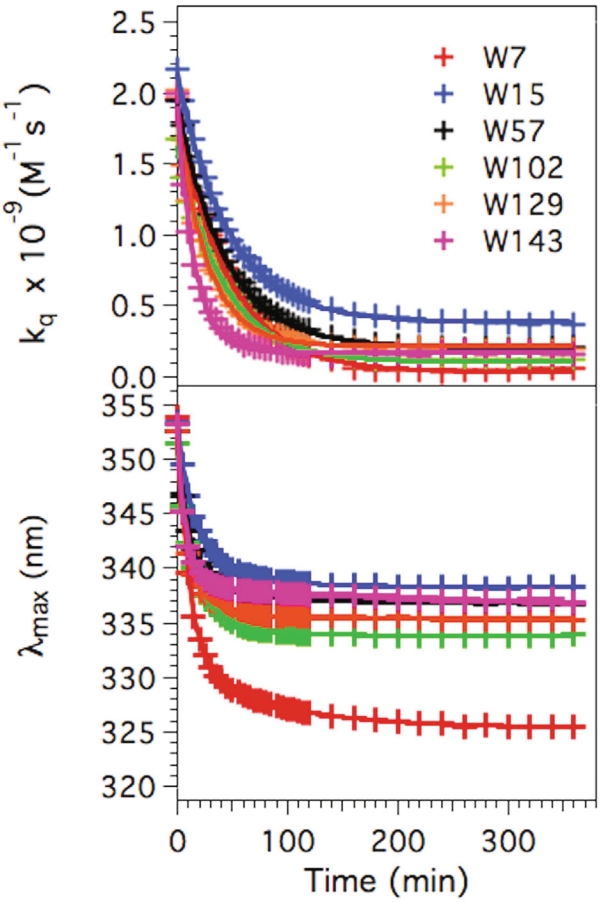

Fig. 4. Evolution of k_q (top panel) and λ_{max} (bottom panel, absence of acrylamide) during the folding reaction of OmpA mutants into SUVs. The values are averages of 3–4 trials. Solid curves are fits to single exponential (top) or double exponential (bottom) functions. The values for k_q were determined from the sphere-of-action model using a fixed V of 0.46 M^{-1}.

the spectra blue-shifted 15–29 nm, from t = 0 h (unfolded) values of 351–354 nm, to t = 6 h (folded) values of 325–338 nm in the absence of acrylamide. The graphs of λ_{max} versus time for the 0.0 M acrylamide samples were fit to single and double exponential functions. A double exponential fit was required, and the resulting fit gave rise to reciprocal time constants of 7–13 min for the fast component and 25–84 min for the slow component for all mutants (Table 2). The exponential fits and residuals are shown in Supporting Information. In the presence of acrylamide, the folding-induced blue-shifts were slightly reduced by about 3 nm; for example, for the representative W102 data in Figs. 2 and 3, the blue-shift in the presence of 0.0, 0.1, 0.2, 0.3, and 0.4 M acrylamide were 17, 16, 15, 15, and 14 nm, respectively.

The correlation between k_q and λ_{max} values is shown in Fig. 5 for each mutant in the following states: denatured in 8.0 M urea, t = 0 h during folding, adsorbed on DPPC, and fully folded at t = 6 h. A general trend of high values of k_q for high values of λ_{max} is observed. The analogous graph for K_D and λ_{max} is shown in Supporting Information.

The permeability and integrity of SUVs in the presence of acrylamide and OmpA were analyzed by leakage assays and DLS measurements. Spectra of ANTS fluorescence for SUVS in the absence and presence of acrylamide are shown in Supporting Information; the presence of acrylamide caused ANTS fluorescence to increase in a pseudo-linear fashion over time. OmpA also caused vesicles to leak, albeit at a slower timescale than acrylamide. The relative kinetics of folding and leakage are compared in Supporting Information; these data indicate that the folding reaction is faster by a factor of 7 compared to leakage caused by acrylamide. Despite the enhanced permeability of SUVs in the presence of acrylamide or OmpA, the integrity of the vesicle is not compromised. DLS analysis indicates that the size of the SUVs is unaffected by the presence of acrylamide or OmpA. The maintenance of an intact vesicle is also evidenced in the OmpA fluorescence data which shows that the scattering component near ~300 nm remains unchanged and only disappears upon lysis with Triton X-100. DLS experiments were also conducted to confirm negligible effects of time and acrylamide on the size of the vesicles.

4. Discussion

OmpA is an integral membrane protein that has served as a model β-barrel system for the study of membrane protein folding for nearly 30 years, since the first report in 1992 [20]. The slow folding rate enables straightforward spectroscopic studies using steady-state methods. The present study aims to elucidate the evolution of protein (de)solvation during the *in vitro* folding reaction of OmpA via fluorescence quenching experiments. Stern-Volmer analysis of OmpA mutants during folding leads to site-specific insights on the accessibility of a quencher, acrylamide, to tryptophan at varying locations within its transmembrane domain. These results complement prior studies that focused on the kinetics and formation of secondary and tertiary structures as well as depth of insertion into the bilayer.

4.1. Acrylamide as the quencher

Acrylamide has been widely used to measure the extent of solvent accessibility for tryptophan. One reason for its utility is that the experiment is simple and involves steady-state or lifetime measurements of tryptophan fluorescence in the presence of different concentrations of acrylamide. The mechanism of quenching has been attributed to electron transfer [30,31,41]. There are static and dynamic contributions to the quenching mechanism, and the presence of both components is evident in the upward curvature of the Stern-Volmer graph of NATA (Supporting Information). In Eq. (3), the constant V is interpreted as the volume element around the fluorophore within which the fluorescence is instantaneously quenched. For NATA in phosphate buffer, a fit of the data to Eq. (3) yields a value of V = 1.4 M^{-1}; this value corresponds to a radius of 8 Å, meaning that an acrylamide molecule within 8 Å of a photoexcited NATA molecule will result in a non-fluorescent, dark form of NATA. In 8.0 M urea, the value of V remains 1.4 M^{-1} while the value of K_D decreased from 14.2 (buffer) to 10.7 (urea) M^{-1}. This change in K_D corresponds to a decrease in k_q from 4.7×10^{-9} to 2.4×10^{-9} M^{-1} s^{-1} using values of τ_0 of 3.0 and 4.5 ns, respectively [40,42]. The decrease in bimolecular quenching constant k_q by a factor of 2 is consistent with the increase in viscosity of a factor of 1.7 for 8.0 M urea compared to buffer [28,43]. There is a slight temperature-dependence of the Stern-Volmer graph that supports the predominantly dynamic nature; with an increase in temperature from room temperature to 37 °C, the value for K_D increased less than 10%.

In proteins with single tryptophan residues, the Stern-Volmer graphs with acrylamide are varied, and both upward-curving and linear graphs, with V typically ranging between 0 and 1.0 M^{-1}, have been reported [29]. For example, values of V = 1.0, 0.6, and 0.0 M^{-1} have been reported for folded glucagon, HSA (in SDS) and for RNase, respectively [29]. The general trend is that protected tryptophan residues in rigid protein environments exhibit linear or pseudo-linear Stern-Volmer graphs, with low or zero values for V

Table 1
Summary of results from Stern-Volmer analysis. The conditions are denatured in 8.0 M urea, aggregated in 0.5 M urea, adsorbed on DPPC SUVs, and during folding into DMPC SUVs (t = 0 hr and t = 6 hr). The change in K_D during folding, K_D (t = 0 hr) – K_D (t = 6 hr), is indicated as ΔK_D folding. The average K_D and k_q values for the six mutants is indicated in the last column. The evolution of K_D and k_q during folding were fit to an exponential function $K_D(t) = Ae^{-t/\tau_{desolv}} + y_0$ or $k_q(t) = Ae^{-t/\tau_{desolv}} + y_0$ using a global analysis of multiple trials. The K_{SV} values at t = 6 hr were determined for each mutant using a global fit to multiple trials. Slight discrepancies in the table reflect rounding outcomes.

OmpA mutant	W7	W15	W57	W102	W129	W143	
$\boldsymbol{K_D}$ (M^{-1})							Avg
denatured[a]	6.3	5.3	6.1	6.9	8.0	5.7	6.4
aggregated[a]	5.9	4.0	5.9	6.4	6.8	6.3	5.9
adsorbed[a]	1.7	2.0	2.0	2.6	1.0	2.1	1.9
t = 0 hr[b]	6.7	7.1	7.7	7.1	7.0	6.3	7.0
t = 6 hr[b]	0.1	1.2	0.8	0.4	0.8	0.5	0.6
ΔK_D folding	6.6	5.9	6.9	6.7	6.2	5.8	6.4
$\boldsymbol{K_D}$ decay parameters[b]							
τ_{desolv} (min)	46 ± 3	46 ± 2	43 ± 4	41 ± 1	27 ± 1	15 ± 1	–
A (M^{-1})	6.6 ± 0.2	5.8 ± 0.1	6.9 ± 0.3	6.7 ± 0.1	6.3 ± 0.2	5.8 ± 0.1	–
y_0 (M^{-1})	0.1 ± 0.1	1.2 ± 0.1	0.8 ± 0.1	0.4 ± 0.1	0.8 ± 0.1	0.5 ± 0.1	–
$\boldsymbol{K_{SV}}$ (M^{-1})[c]							Avg
t = 6 hr	0.7	1.9	1.4	1.1	1.3	1.1	1.3
$\boldsymbol{k_q}$ (10^{-9} $M^{-1}s^{-1}$)[d]							Avg
denatured	2.0	1.8	1.8	1.8	2.4	2.0	2.0
aggregated	1.9	1.4	1.7	1.6	2.0	2.2	1.8
adsorbed	0.5	0.6	0.5	0.6	0.3	0.7	0.5
t = 0 hr	1.9	2.1	1.9	1.6	1.9	1.9	1.9
t = 6 hr	0.02	0.4	0.2	0.1	0.2	0.2	0.2
$\boldsymbol{k_q}$ decay parameters[e]							
τ_{desolv} (min)	46 ± 3	46 ± 2	43 ± 4	41 ± 1	27 ± 1	15 ± 1	–
A (10^{-9} $M^{-1}s^{-1}$)	1.8 ± 0.1	1.8 ± 0.1	1.7 ± 0.1	1.5 ± 0.1	1.7 ± 0.1	1.8 ± 0.1	–
y_0 (10^{-9} $M^{-1}s^{-1}$)	0.02 ± 0.03	0.38 ± 0.02	0.20 ± 0.03	0.09 ± 0.01	0.20 ± 0.01	0.16 ± 0.01	–

[a] Values for V were 0.80 M^{-1}, 0.71 M^{-1}, and 0.39 M^{-1} for denatured, aggregated, and adsorbed OmpA, respectively. The error for K_D values is 8% and were derived from the sphere-of-action fits (n = 1 for each condition).
[b] Values for K_D at t = 0 and 6 hr were determined from the resulting parameters of the fit with V fixed at 0.46 M^{-1}. The errors for K_D decay parameters are derived from global fits to multiple trials for the folding reaction (n = 3 for W7, W57, W102, W129, W143; n = 4 for W15).
[c] The errors for K_{SV} are 10% (W7), 5% (W15), 6% (W57), 6% (W102), 11% (W129), 8% (W143) and were derived from global fits to the same trials to determine K_D.
[d] The average of the tryptophan lifetime, τ_0^{avg}, in urea and DMPC, for each OmpA mutant was used to calculate corresponding k_q values for t = 0 hr, t = 6 hr, and adsorbed states; the values for τ_0^{avg} were 3.6 ns (W7), 3.3 ns (W15), 4.0 ns (W57), 4.4 ns (W102), 3.8 ns (W129), 3.3 ns (W143). The known values of τ_0 in urea were used to calculate k_q for the denatured and aggregated states. The lifetimes were obtained from reference 44.
[e] The errors for k_q decay parameters were derived from global fits to the same trials to determine K_D.

Table 2
Summary of results from wavelength analysis. The conditions are denatured in 8.0 M urea, aggregated in 0.5 M urea, adsorbed onto DPPC SUVs, and during folding (extrapolated at t = 0 hr and t = 6 hr). The change in λ_{max} during folding, λ_{max} (t = 0 hr) – λ_{max} (t = 6 hr), is indicated as $\Delta\lambda_{max}$ folding. The evolution of λ_{max} during folding were fit to a double exponential function $\lambda_{max}(t) = A_{fast}e^{-t/\tau^{fast}_{environment}} + A_{slow}e^{-t/\tau^{slow}_{environment}} + y_0$ using a global analysis to multiple trials. Stated errors for the kinetic fits are upper and lower limits for multiple trials. Slight discrepancies in the table reflect rounding outcomes.

OmpA mutant	**W7**	**W15**	**W57**	**W102**	**W129**	**W143**
λ_{max} (nm)						
denatured[a]	356	355	355	355	356	355
aggregated[a]	353	352	352	351	353	353
adsorbed[a]	339	339	342	342	333	342
t = 0 hr[b]	354	353	352	351	352	353
t = 6 hr[b]	325	338	337	334	335	337
$\Delta\lambda_{max}$ folding	29	15	15	18	17	16
Decay parameters[b]						
$\tau^{fast}_{environment}$ (min)	11 ± 1	13 ± 3	9 ± 1	8 ± 2	7 ± 1	7 ± 1
$\tau^{slow}_{environment}$ (min)	84 ± 32	48 ± 21	48 ± 12	25 ± 4	28 ± 8	80 ± 21
A_{fast} (nm)	23 ± 2	11 ± 3	12 ± 1	9 ± 2	13 ± 2	14 ± 1
A_{slow} (nm)	6 ± 1	4 ± 3	4 ± 1	9 ± 2	4 ± 2	2 ± 1
y_0 (nm)	325 ± 1	338 ± 1	337 ± 1	334 ± 1	335 ± 1	337 ± 1

[a] The error for λ_{max} values for denatured, aggregated, and adsorbed OmpA is 0.1% based on the error of the Gaussian fit to the fluorescence curve of the 0.0 M acrylamide samples (n = 1 for each condition).
[b] Values for λ_{max} at t = 0 and 6 hr were determined from the resulting parameters of the fit. The error for λ_{max} decay parameters were derived from global fits to multiple trials for the folding reaction (n = 3 for W7, W57, W102, W129, W143; n = 4 for W15).

and low values of k_q while solvent-exposed and dynamic tryptophan residues exhibit upward curvature and relatively high values of V and k_q. In exceptional cases, a protein may exhibit a large V, indicative of high probability of finding acrylamide near tryptophan, but with a small k_q, indicative that the tryptophan is buried and protected by the protein; this seemingly contradictory situation has been explained by considering the dynamics of the protein where relatively high concentration of acrylamide may be found near an otherwise protected tryptophan because of favorable protein dynamics and thermodynamics that creates a high local concentration of acrylamide [44]. Unfolded proteins with a solvent-exposed tryptophan generally exhibit curved Stern-Volmer graphs,

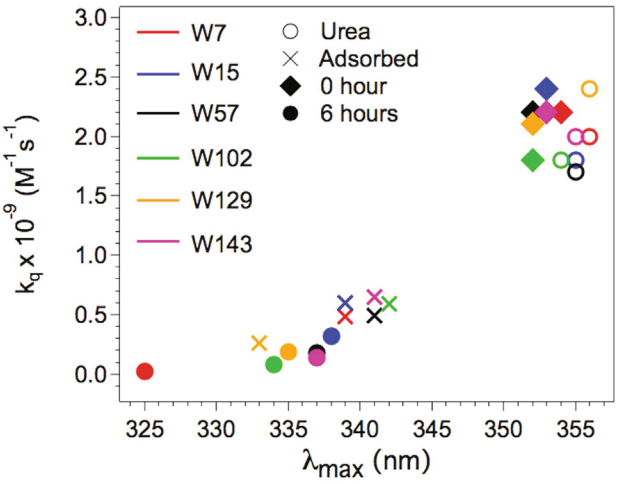

Fig. 5. Correlation of average values of k_q and λ_{max} for different conformations of OmpA: denatured in 8.0 M urea, adsorbed on DPPC SUVs, t = 0 h during folding into DMPC SUVs, and fully folded in DMPC SUVs at t = 6 hrs. The values are from Tables 1 and 2.

with values of V around 0.7–0.9 M^{-1} [29,45], e.g. for the unfolded TN-I subunit (V = 0.7 M^{-1}) and β-trypsin (V = 0.9 M^{-1}) [29,45]. Some proteins, such as pepsin and β-trypsin, exhibit linear Stern-Volmer graphs in the folded form that evolve to a positive-curvature graph upon unfolding [29]. For proteins with multiple tryptophan residues, downward-curving Stern-Volmer graphs that reflect fractional accessibility of fluorophores are also possible [28].

The Stern-Volmer graphs of OmpA evolve during folding: they have upward curvature for denatured protein and in the initial stages of folding, and are linear at a later stage of folding and for fully folded protein. The systematic loss of curvature is reasonable and may reflect the impact of the change in local environment of the tryptophan residue during folding. For example, the quenching mechanism may be less efficient in a bilayer environment and thus, the value of V could decrease as the protein folds. On the other hand, an alternative analysis would assume the value of V is essentially constant for a given tryptophan because the quenching mechanism is primarily defined by the inherent properties of the tryptophan-acrylamide pair for a protein, and not necessarily the local environment. We have adopted the latter strategy and maintained a constant value of V for all mutants during folding. This seemed the most reasonable approach because of the limited dataset and lack of rigorous constraints that would allow simultaneous optimization of V and K_D in a reasonable manner for all timepoints. Thus, we have taken two approaches to analyze the Stern-Volmer graphs. In the first approach, all Stern-Volmer graphs were analyzed using a constant value of V and corresponding decay constants for the evolution of K_D during folding were determined for a given value of V. Four different values of V that encompass the range reported for other proteins ($V = 0.0, 0.3, 0.6, 0.9$ M^{-1}) were tried. In the second approach, an average value of V based on our experimental data was utilized. This average value was determined from a global fit to all 38 Stern-Volmer graphs for the six mutants, as described above. The resulting global average value of V = 0.46 M^{-1} is consistent with other values of V from literature. The results from both methods are discussed below.

4.2. Bimolecular quenching and local environment for tryptophan in various OmpA conformations

OmpA mutants that contain single tryptophan residues were studied in different equilibrium conformations, including denatured in 8.0 M urea, adsorbed on DPPC SUVs, aggregated in 0.5 M urea, and folded in DMPC SUVs. A summary of the Stern-Volmer constants (K_D) and emission maxima (λ_{max}) are provided in Tables 1 and 2. In general, the sphere-of-action K_D values exhibited a trend of $K_D^{denatured}(6.4\ M^{-1}) > K_D^{aggregated}\left(5.9\ M^{-1}\right) > K_D^{adsorbed}(1.9\ M^{-1}) > K_D^{folded}(0.6\ M^{-1})$, where the parenthetical values are the average value of K_D for all six mutants. An additional value of interest is the extrapolated values of K_D at the first time point (t = 0 hr) during folding; these values ranged from 6.3 to 7.7 M^{-1} for the six mutants (average value of 7.0 M^{-1} for all six mutants). The corresponding values for k_q are included in Table 1. The general trend of decreasing k_q during folding is accompanied by the blue-shift of λ_{max}; Fig. 5 shows a correlation between k_q and λ_{max} where folded OmpA exhibits the lowest values of k_q and most blue-shifted λ_{max} (~330 nm) while denatured protein has the highest values of k_q and most red-shifted λ_{max} (~355 nm).

The Stern-Volmer results are comparable to prior Stern-Volmer studies of OmpA in the denatured, aggregated, adsorbed, and folded conformations [33,34,46]. These previous studies focused on wild-type OmpA and thus, the results reflect an average of the five native tryptophan residues. These prior studies did not utilize a Stern-Volmer model that reflects a combined static and dynamic quenching mechanism despite the upward curvature for the denatured and aggregated species. Nonetheless, the Stern-Volmer graphs of the denatured conformation reported here are similar to these prior studies in terms of relatively high values of F_0/F as a function of acrylamide concentration as well as the positive curvature; in the present experiments, V = 0.80 M^{-1} for denatured protein in 8.0 M urea. The emission maxima of the tryptophan residues in denatured OmpA (354–356 nm) are also comparable to all previous reports and also similar to NATA in 8.0 M urea. The Stern-Volmer constants and emission maxima for the t = 0 hr unfolded structure at the initial stage of folding are similar to those of the denatured state in terms of the emission maxima and K_D values.

4.3. Aggregation

The aggregated state, defined as OmpA in 0.5 M urea, represents a potential competitive, stable species that prevents folding into bilayers [20]. The structure of aggregated OmpA has been reported to be a mixture of α-helix and β-strand in the periplasmic domain and unstructured in the transmembrane β-barrel region based on circular dichroism [20,47]. This species may be relevant to the present study because the folding reaction is initiated by rapid dilution of a stock solution of denatured OmpA in 8.0 M urea to a final urea concentration of 0.5 M in the presence of SUVs. Thus, it is possible that some population of OmpA may aggregate and prevent folding into SUVs. There is a modest blue-shift of the emission maxima of 2–3 nm (from average of 355 nm to 352 nm for all mutants) compared to the denatured state. There is also a minor decrease in the K_D values to a range of 6.8–4.0 M^{-1} (average value of 5.9 M^{-1} for all mutants) relative to denatured state. The positive curvature of the Stern-Volmer curves for the aggregated state is reflected in V = 0.71 M^{-1}, which is also similar to the denatured state value of V = 0.80 M^{-1}. These results do not evolve within the time resolution of the present experiments and indicate that the aggregated and denatured states exhibit similar quenching behavior. There is one previous experiment on the aggregated state of wild-type OmpA; however, this previous study utilized a linear quenching model and reported a low-temperature Stern-Volmer constant of 5.3 M^{-1} (0.08 M urea at 2 °C) [33]. This study also illustrated that the Stern-Volmer constant is relatively high, and more similar to denatured protein than to folded protein.

The observation that the tryptophan residues experience similar levels of solvent accessibility and local environment in the

aggregated and denatured states is consistent with the nature of OmpA. Like many β-barrel membrane proteins, OmpA is not highly hydrophobic and therefore, is not expected to aggregate as easily as the hydrophobic, alpha-helical membrane proteins [48,49]. Despite the potential for an aggregated state to serve as an off-pathway intermediate in the folding process, there is no evidence of such a folding trap in the present studies. First, prior studies of OmpA folding with gels, which monitors the formation of tertiary structure, illustrated that under these conditions, OmpA folds with 80–97% efficiency [20,25,50]. Additionally, decomposition of the fluorescence spectra in our studies of the fully folded species (t = 6 h) indicates 78–100% folding efficiency across all mutants. Finally, the Stern-Volmer graphs of OmpA during folding indicate that the extrapolated values of K_D at the earliest timepoint of 0 hr is relatively large (6.3 – 7.7 M^{-1}), similar to the values of aggregated and denatured states. Thus, if an aggregated state exists, it does not appear to be prohibiting the folding process in the current experiments.

4.4. Adsorption

The adsorbed state represents a potential on-path intermediate during folding. In the present experiments, the adsorbed state was prepared by incubating OmpA with DPPC SUVs at room temperature; under this condition, the DPPC bilayer is in the gel phase, and thus has greater thickness and is more rigid than fluid-phase DMPC bilayers, preventing folding and insertion into the bilayer [51]. The adsorbed species exhibits β-barrel features similar to the native state based on circular dichroism studies, and there appears to be greater secondary structure for the partially inserted adsorbed state than aggregated state [20,52]. In the current report, the results suggest that the adsorbed conformation has tryptophan residues that are more protected from the solvent (less steep and less curved Stern-Volmer graph) and in a more hydrophobic environment (blue-shifted emission maxima) relative to the denatured and aggregated states. As with the aggregated state, the spectral features of the adsorbed state do not evolve with time and the adsorbed species appears to be formed within a few seconds of mixing OmpA with DPPC SUVs. The previously reported linear Stern-Volmer constants for the adsorbed state of 2.8 M^{-1} (adsorbed on DMPC vesicles at 10 °C) [34] and 5.4 M^{-1} (adsorbed on DOPC vesicles at 2 °C) [33] are higher than the values reported here, but this systematic difference can be attributed to the use of a sphere-of-action model in the present study that leads to K_D values of 1.0–2.6 M^{-1}. Temperature effects may also impact the quenching data.

4.5. Folding

The fully folded structures exhibit the most buried and hydrophobic environments for all six single-tryptophan mutants. The Stern-Volmer graphs for folded species appear linear and with the smallest slope; the prior reports of 2.2 M^{-1} (folded in DMPC vesicles at 30 °C) [34] and 1.8 M^{-1} (folded in DOPC vesicles at 40 °C) [33] are higher than the sphere-of-action K_D values in the present study 0.1 to 1.2 M^{-1}. However, if a linear as opposed to sphere-of-action fit to the Stern-Volmer graphs for the six OmpA mutants is utilized here, the resulting K_{SV} values of 0.7–1.9 M^{-1} are comparable to previous reports (Table 1). The decrease in Stern-Volmer constants translates directly to decreased bimolecular quenching constants (k_q) by about a factor of 10, perhaps more, for the folded state compared to denatured state. The decrease in bimolecular quenching constant is consistent with the increased viscosity in the fluid DMPC lipid bilayer ($T > T_m$) by a factor of 40 compared to in 8.0 M urea [43,53]. The fact that the bimolecular quenching constant remains relatively high for some mutants, such as W15 with K_D = 1.2 M^{-1} suggests that some tryptophan residues are accessible to solvent, or perhaps are dynamic, in the folded state.

4.6. Evolution of bimolecular quenching and local environment during folding

The expected evolution of V during folding led to different methods to analyze the Stern-Volmer kinetics. In the simple approach, four different values of V from 0.0 to 0.9 M^{-1} were tried for each mutant; this range encompasses published values of V for other proteins and also encompasses the maximum and minimum value of V for any OmpA mutant. In a more informed approach, a single average value of V = 0.46 M^{-1} based on a global fit to all trials of OmpA t = 0 and 6 hr timepoints was utilized. Both analyses gave the same result for reciprocal decay constant within error. Thus, we will focus on the values with V = 0.46 M^{-1}.

A reasonable hypothesis is that the K_D values (and hence k_q) should decrease during folding because the tryptophan residues become buried and inaccessible by the acrylamide quencher. The data support this hypothesis. The temporal evolution of K_D could be satisfactorily modeled with an exponential function (Table 1); use of a double exponential function did not improve the fits substantially (Supporting Information). The values of k_q for the earliest time point during folding (t = 0 hr) were extrapolated using the parameters from the exponential fit; these k_q values for the six mutants varied 1.6–2.1 × 10^{-9} M^{-1} s^{-1}, which are similar to those of the denatured state. The similarity of k_q values for the denatured state and at t = 0 hr is consistent with the observation that the denatured state is expanded, and that folding competes successfully against aggregation/oligomerization [47]. The $k_q$values decrease substantially in the folded state (0.02–0.4 × 10^{-9} M^{-1} s^{-1}). The inverse decay constants ($1/k$) for the evolution of k_q during folding, referred to as desolvation lifetimes ($\frac{1}{k} = \tau_{desolv}$), were 41–46 min (W7, W15, W57, W102), 27 min (W129), and 15 min (W143). This variation suggests there is site-specific desolvation kinetics associated with folding, discussed below.

A kinetic analysis of the evolution of emission maxima was also performed, and the results are presented in Table 2. It is well documented that the emission maxima of the tryptophan residues in OmpA undergo a blue-shift during folding. This blue-shift has been interpreted as a change in local environment from aqueous (unfolded and at early time) to hydrophobic (fully folded). In contrast to the decay of k_q, the temporal evolution of λ_{max} exhibited fast and slow components and required a double exponential function (Supporting Information). The fit parameters from the double exponential fit were used to extrapolate values of λ_{max} at the earliest time during folding (t = 0 hr). The magnitude of the blue-shift during folding was mutant-dependent. W7 exhibited the largest shift of 29 nm while other mutants shifted 15–18 nm. This blue-shift has been previously reported by other studies of the OmpA mutants in DOPC vesicles at 40 °C [26] as well as in DMPC at 37 °C [54]; in both of these prior reports, the value of λ_{max} at t = 0 hr were not extrapolated through kinetic fits. The fast and slow inverse rate constants, $\tau^{fast}_{environment}$ amd $\tau^{slow}_{environment}$, were 7–13 min and 25–84 min, respectively. The fast component accounts for the majority (50–80%) of the blue shift.

The kinetics of the blue-shift differ from those of the change in emission intensity at a fixed wavelength of 332 nm. The latter reflects a combination of evolution of the wavelength and fluorescence quantum yield, and has been shown to scale linearly with population of folded protein in a two-state model. The evolution of the emission intensity was analyzed and compared to the kinetics of the blue-shift; the rate constants associated with intensity

changes were slower by a factor of 1.5 – 3.2 than those of the rate constants for the blue shift; $\tau^{fast}_{intensity332nm}$ was 10–25 min and $\tau^{slow}_{intensity332nm}$ was 28–117 min (data not shown). These kinetics of intensity increase are consistent with prior reports [26,33,55].

Previous folding studies of OmpA mutants in DOPC vesicles at 2 °C reported similar decay constants from double exponential fits to the fluorescence data [26]. In this previous study, the fast component (τ_{fast} = 1.4–1.8 min) of the evolution of the fluorescence intensity was attributed to adsorption of OmpA to the bilayer surface, and the slower component was attributed to transition from the adsorbed state to a partially folded and inserted intermediate. Other time- resolved studies probed the formation of secondary [56] and tertiary [27,56,57] structures. A circular dichroism study on the folding of a truncated (absence of periplasmic domain) OmpA mutant into DMPC SUVs revealed a time of 37 min for the formation of the β- structure of the transmembrane domain (data not published). Another circular dichroism study of OmpA folding into a shorter chain lipid $di C_{12}PC$ showed a first- and second- order rates of 20 and 12 min, respectively [56]. It is expected that the folding rate increases with decreasing lipid chain length [56]. The time of 37 min for formation of β-structure during folding into DMPC SUVs is comparable to τ_{desolv} and $\tau^{slow}_{environment}$ reported here, which suggests that desolvation may be involved in the formation of secondary structure. The formation of tertiary structure was probed by Förster resonance energy transfer (FRET) experiments that determined changes in the distance between a tryptophan FRET donor and a cysteine-linked FRET acceptor dye molecule over the time of the folding reaction [57]. For a donor/acceptor pair at positions 7 and 129 (directly across the pore on the periplasmic side) these studies determined that a rapid collapse occurs within 2 min and the majority of pore formation is complete after 50 min [57]. A final set of complementary data come from fluorescence quenching experiments with brominated lipids in the bilayer [33]. These experiments were conducted at 2 °C and probed the movement of the trytophan residues along the bilayer normal, and revealed two timescales of 2 min for the first, fast transition that was attributed to adsorption onto the bilayer, and 87 min for the second, slow transition attributed to insertion [33]. The slow time component from this experiment is similar to $\tau^{slow}_{environment}$ for W7 and W143. These previous experiments support fast and slow components in the folding pathway.

Additional insights are provided through comparison of the evolution of λ_{max} and k_q. With the exception of W102, which is the only tryptophan mutant that does not point towards the bilayer in the published structures, the general trend for the five lipid-facing mutants is

$$\tau^{fast}_{environment}(7-13\ \text{min}) < \tau_{desolv}(15-46\ \text{min}) \leq \tau^{slow}_{environment}(25-84\ \text{min})$$

. The different kinetics associated with evolution of λ_{max} and k_q indicates that there is a fast change in λ_{max} that precedes the change in solvent accessibility (k_q), followed by a comparable or slower equilibration reflected in continuous evolution of λ_{max}. This result can be restated as the majority of the change in environment (blue-shift) occurs in a fast step, while the desolvation process (collisional quenching) occurs in a slower step.

These results augment previous findings. We propose that the fast step revealed by λ_{max} reflects a transition from a fully solvent exposed, extended, unfolded conformation to a different conformation in which the tryptophan residues are in a less polar environment in the polar head group region of the lipid bilayer, where acrylamide continues to exist. The existence of acrylamide in the headgroup region is reasonable based on consideration of the relevant dielectric constants. Water has a dielectric constant of about 74 at 37 °C [58], and the dielectric constants associated with the bilayer is about 23–40 (phosphatidylcholine polar headgroup region) [59,60] and 2 (lipid core) [61,62]. The dielectric constant of acrylamide has been estimated to be around 43; this value was calculated by a proportional estimate from dielectric constants of acetamide in solid (dielectric of 4) [63] and liquid forms (dielectric 59) [63] and a dielectric constant for solid acrylamide of 2.9 [64]. The moderately polar region of the bilayer headgroup favorably accommodates the tryptophan residues and acrylamide when OmpA initially associates with the lipid bilayer, and this association would result in the observed blue-shift of emission maxima but relatively high accessbility of acrylamide to tryptophan. The fast component is therefore attributed to a transition of OmpA from a solvent exposed, unfolded state with large k_q and ~352 λ_{max} values to a partially inserted adsorbed state in the bilayer headgroup that has a decreased dielectric constant (blue-shifted λ_{max}) but relatively high acrylamide concentration (large k_q). This conclusion is consistent with the results of brominated quenching experiments that determined the distance of the tryptophan residues in the first membrane-bound intermediate to be ~14–16 Å from the center of the DOPC lipid bilayer, a distance that is consistent with the polar region of the bilayer [33,65]. It is important to note that this initial, on-path adsorbed structure is likely different from the trapped adsorbed species that is isolated with DOPC. The reason for this distinction is because the values for K_D are much larger for the t = 0 hr intermediate compared to the isolated adsorbed species.

The two comparable slow components, $\tau_{desolv}(15-46\ \text{min})$ and $\tau^{slow}_{environment}(25-84\ \text{min})$, are attributed to a transition of the trp residues from the polar region of the lipid bilayer into the hydrophobic core of the bilayer, resulting in concomitant decrease in k_q and further blue-shifting of λ_{max} to the fully folded values. The kinetics of intensity changes, $\tau^{fast}_{intensity332nm}(10-25\ \text{min})$ and $\tau^{slow}_{intensity332nm}(28-117\ \text{min})$, are also comparable to these slow events. The slow transition also occurs on roughly the same timescale as formation of secondary and tertiary structures, thus supporting the previously proposed concerted mechanism of folding. The fact that the K_D values of folded OmpA are not zero can be explained by the presence of acrylamide in the bilayer itself [66].

4.7. Vesicle integrity

Control experiments were performed to confirm that the observed quenching reflects structural changes of OmpA as opposed to loss of vesicle integrity on account of acrylamide. These experiments are important because it has been shown that acrylamide and other small molecules can diffuse through lipid bilayers [66,67] and it is not clear if this diffusion alters the vesicle properties. The control experiments involved leakage assays in which FRET donor and acceptor molecules (ANTS and DPX, respectively) were encapsulated within the interior of the SUVs, and if released to the extravesicular space, the FRET donor produced a large fluorescence signal. The data show that in the presence of 0.4 M acrylamide or OmpA, the DMPC SUVs leaked at a faster rate than in the absence of acrylamide or protein, indicating that acrylamide and OmpA cause vesicles to be more permeable. However, the leakage rate as assessed by the increase in fluorescence from ANTS was much slower than the folding kinetics. The $1/e$ time for the change in ANTS fluorescence in the presence of acrylamide is 260 min while the $1/e$ times for K_D and λ_{max} are at least 6-fold faster (5–40 min). In the presence of OmpA, the leakage was substantially slower ($1/e$ time of 700 min) and the inherent degradation of the SUVs was negligible. Despite the leakage caused by acrylamide, the SUVs remained intact. DLS and fluorescence data indicate that the size (~50 nm) and scattering properties of the SUVs were

unchanged in the presence of acrylamide. This observation is important because OmpA has been shown to fold and insert into highly curved SUVs and not into lower-curvature large unilamellar vesicles [18,20].

4.8. Implications for folding: Site specific mutants

The present study provides insights into site-specific changes in k_q and λ_{max} values during the folding reaction. The smallest value of k_q and most blue-shifted λ_{max} was observed for W7. This result indicates that for folded OmpA, the tryptophan residue at position 7 is in the most hydrophobic environment of the lipid region with least amount of bimolecular quenching relative to all six tryptophan residues studied here. The largest value of k_q and least blue-shifted λ_{max} was observed for W15. This result for W15 is consistent with the reported interaction between the tryptophan at position 15 and the lipid head group; for example, UV resonance Raman spectroscopy suggested a cation-π interaction [54,68].

The overall trends of λ_{max} and k_q values for all the mutants are roughly the same, as shown in Fig. 5. A similar correlation between λ_{max} and the Stern-Volmer constant has been reported in a prior study of melittin [69]. In OmpA, the λ_{max} trend is: W7 (325 nm) < W102 (334 nm) < W129 (335 nm) < W143 (337 nm) ≈ W57 (337 nm) < W15 (338 nm). Previous data for λ_{max} of single-trp mutants of OmpA (except W129) in DMPC and DOPC vesicles showed the similar trend, although there was slight variation in the actual values of λ_{max} [26,40,54]. The k_q trend is: W7 (0.02×10^{-9} M^{-1} s^{-1}) < W102 (0.1×10^{-9} M^{-1} s^{-1}) < W129 (0.2×10^{-9} M^{-1} s^{-1}) ≈ W143 (0.2×10^{-9} M^{-1} s^{-1}) ≈ W57 (0.2×10^{-9} M^{-1} s^{-1}) < W15 (0.4×10^{-9} M^{-1} s^{-1}). The result for W102 is interesting because according to two structures, the tryptophan residue at position 102 faces the interior of the pore (X-ray) or the extravesicular region (NMR) instead of towards the lipid bilayer [21,22]; thus, one might expect a less hydrophobic environment and facile solvent accessibility and hence, more red-shifted λ_{max} and higher value for k_q than is reported here. The hydrophobic environment and inaccessibility of acrylamide to quench the tryptophan residue at position 102 suggests that the detergent-solubilized crystal and NMR structures may differ from the bilayer-solubilized structure. An alternative interpretation is that the protein dynamics in this region of the protein restrict solvent accessibility.

The kinetics of folding also exhibit site-specific behavior. W143 exhibits the fastest decrease in solvent accessibility ($\tau_{desolv} = 15$ min), followed by W129 ($\tau_{desolv} = 27$ min). The remaining mutants exhibit similar values of τ_{desolv} of 41–46 min. The blue-shift of λ_{max} is also fastest for W143 and W129, though the values for $\tau^{fast}_{environment}$ have larger errors and are within a factor of two for all the mutants. The fast desolvation process of the tryptophan residues at positions 143 and 129 may reflect a more rapid entry into the bilayer. However, a previous study suggested that the four tryptophan residues at positions 15, 57, 102, and 143 transverse the bilayer at similar rates in the concerted mechanism of folding. An alternative explanation is that the desolvation process is more facile near positions near 143 and 129, in part because of their relative proximity in sequence to the soluble tail. The transmembrane portion nominally ends at residue 171, and the soluble tail has been hypothesized to serve as a chaperone that prevents undesireable oligomerization of OmpA [47]. Residues near the soluble tail may be more rapidly desolvated through interactions with the chaperone-like tail.

5. Conclusion

Fluorescence quenching studies with acrylamide on six OmpA mutants has probed site-specific desolvation kinetics and changes in local tryptophan environment in the transmembrane domain upon folding into lipid bilayers. The use of single-tryptophan OmpA mutants for site-specific investigations during folding are an improvement to previous quenching studies which utilized wild-type OmpA and probed the average of the five native tryptophan residues in equilibrium conformations. The improved Stern-Volmer analysis for OmpA folding uses the sphere-of-action model which reflects both static and dynamic components in the quenching mechanism to account for the upward curvature associated with some conformations. As OmpA transitions from an unfolded conformation at the earliest time point of the folding reaction to its native state within the bilayer, the loss of accessibility of acrylamide to tryptophan is reflected by the exponential decrease in K_D over time. The present results complement and support previous studies that suggest a concerted OmpA folding mechanism.

CRediT Author Statement

D.K.A contributed to data curation, formal analysis, investigation, writing-original draft and review & editing. I.A.K. contributed to data curation, formal analysis, investigation, writing-original draft. I.L.-P. contributed to formal analysis and writing-review and editing. J.E.K. is the corresponding author and supervised this project. All authors have given approval to the final version of the manuscript.

Declaration of Competing Interest

The authors declare that they have no known competing financial interests or personal relationships that could have appeared to influence the work reported in this paper.

Acknowledgements

We are grateful to Prof. Douglas Magde for the DLS measurements. D.K.A. acknowledges the UCSD NIH Molecular Biophysics Training grant (NIH T32 GM008326) and the UCSD Inamori Graduate Fellowship for support. I.L.-P. acknowledges the UCSD NIH Molecular Biophysics Training grant (NIH T32 GM008326) and the Department of Education Graduate Assistance in Areas of National Need (GAANN) Fellowship. We are grateful for support from the National Science Foundation (CHE-2004081).

Author contributions

D.K.A and I.A.K contributed equally to this manuscript. I.L.-P. contributed to data analysis. J.E.K is the corresponding author and supervised this project. All authors have given approval to the final version of the manuscript.

Appendix A. Supplementary material

Supplementary data to this article can be found online at https://doi.org/10.1016/j.saa.2021.119919.

References

[1] M.S. Cheung, A.E. Garcia, J.N. Onuchic, Protein folding mediated by solvation: water expulsion and formation of the hydrophobic core occur after the structural collapse, Proc. Natl. Acad. Sci. U.S.A. 99 (2002) 685–690.
[2] G.A. Papoian, J. Ulander, P.G. Wolynes, Role of water mediated interactions in protein-protein recognition landscapes, J. Am. Chem. Soc. 125 (30) (2003) 9170–9178.
[3] K.A. Dill, Dominant forces in protein folding, Biochemistry 29 (31) (1990) 7133–7155.
[4] J. Juneja, J.B. Udgaonkar, NMR studies of protein folding, Curr. Sci. 84 (2003) 157–172.

[5] M. Maurer, C. Oostenbrink, Water in protein hydration and ligand recognition, J. Mol. Recognit. 32 (12) (2019), https://doi.org/10.1002/jmr.v32.1210.1002/jmr.2810.
[6] N.A. Krylov, V.M. Pentkovsky, R.G. Efremov, Nontrivial behavior of water in the vicinity and inside lipid bilayers as probed by molecular dynamics simulations, ACS Nano. 7 (10) (2013) 9428–9442.
[7] R. Barnes, S. Sun, Y. Fichou, F.W. Dahlquist, M. Heyden, S. Han, Spatially heterogeneous surface water diffusivity around structured protein surfaces at equilibrium, J. Am. Chem. Soc. 139 (49) (2017) 17890–17901.
[8] R. Chen, W. Schmidmayr, C. Kramer, U. Chen-Schmeisser, U. Henning, Primary structure of major outer membrane protein II (ompA protein) of *Escherichia coli* K-12, Proc. Natl. Acad. Sci. U.S.A. 77 (8) (1980) 4592–4596.
[9] H. Vogel, F. Jähnig, Models for the structure of outer-membrane proteins of *Escherichia coli* derived from raman spectroscopy and prediction methods, J. Mol. Biol. 190 (2) (1986) 191–199.
[10] K.M. Sanchez, J.E. Gable, D.E. Schlamadinger, J.E. Kim, Effects of tryptophan microenvironment, soluble domain, and vesicle size on the thermodynamics of membrane protein folding: lessons from the transmembrane protein OmpA, Biochemistry 47 (2008) 12844–12852.
[11] A.T. Boags, F. Samsudin, S. Khalid, Binding from both sides: TolR and full-length OmpA bind and maintain the local structure of the E. coli cell wall, Structure 27 (2019) 713–724.e2.
[12] I. Sonntag, H. Schwarz, Y. Hirota, U. Henning, Cell envelope and shape of *Escherichia coli*: multiple mutants missing the outer membrane lipoprotein and other major outer membrane proteins, J. Bacteriol. 136 (1978) 280–285.
[13] J. Bosák, L. Micenková, M. Doležalová, D. Šmajs, Colicins U and Y inhibit growth of *Escherichia coli* strains via recognition of conserved OmpA extracellular loop 1, Int. J. Med. Microbiol. 306 (7) (2016) 486–494.
[14] T. Chai, J. Foulds, Demonstration of a missing outer membrane protein in tolG mutants of *Escherichia* cell, J. Mol. Biol. 85 (1974) 465–474.
[15] L.V. Alphen, L. Havekes, B. Lugtenberg, Major outer membrane protein d of *Escherichia coli* K 12, FEBS Lett. 75 (1-2) (1977) 285–290.
[16] D.B. Datta, B. Arden, U. Henning, Major proteins of the *Escherichia coli* outer cell envelope membrane as bacteriophage receptors, J. Bacteriol. 131 (1977) 821–829.
[17] M. SCHWEIZER, I. HINDENNACH, W. GARTEN, U. HENNING, Major proteins of the *Escherichia coli* outer cell envelope membrane. Interaction of protein II* with lipopolysaccharide, Eur. J. Biochem. 82 (1) (1978) 211–217.
[18] T. Surrey, F. Jähnig, Kinetics of folding and membrane insertion of a β-barrel membrane protein, J. Biol. Chem. 270 (47) (1995) 28199–28203.
[19] J.H. Kleinschmidt, Folding of β-barrel membrane proteins in lipid bilayers - Unassisted and assisted folding and insertion, Biochim. Biophys. Acta 1848 (9) (2015) 1927–1943.
[20] T. Surrey, F. Jahnig, Refolding and oriented insertion of a membrane protein into a lipid bilayer, Proc. Natl. Acad. Sci. U.S.A. 89 (16) (1992) 7457–7461.
[21] A. Pautsch, G.E. Schulz, High-resolution structure of the OmpA membrane domain1, J. Mol. Biol. 298 (2) (2000) 273–282.
[22] A. Arora, F. Abildgaard, J.H. Bushweller, L.K. Tamm, Structure of outer membrane protein A transmembrane domain by NMR spectroscopy, Nat. Struct. Mol. Biol. 8 (2001) 334–338.
[23] K. Dornmair, H. Kiefer, F. Jähnig, Refolding of an integral membrane protein. OmpA of *Escherichia coli*, J. Biol. Chem. 265 (31) (1990) 18907–18911.
[24] C.L. Pocanschi, J.-L. Popot, J.H. Kleinschmidt, Folding and stability of outer membrane protein A (OmpA) from *Escherichia coli* in an amphipathic polymer, amphipol A8–35, Eur. Biophys. J. 42 (2-3) (2013) 103–118.
[25] D.K. Asamoto, G. Kang, J.E. Kim, Folding of the beta-barrel membrane protein OmpA into nanodiscs, Biophys. J. 118 (2020) 403–414.
[26] J.H. Kleinschmidt, T. den Blaauwen, A.J.M. Driessen, L.K. Tamm, Outer membrane protein A of *Escherichia coli* inserts and folds into lipid bilayers by a concerted mechanism, Biochemistry 38 (16) (1999) 5006–5016.
[27] G. Kang, I. López-Peña, V. Oklejas, C.S. Gary, W. Cao, J.E. Kim, Förster resonance energy transfer as a probe of membrane protein folding, Biochim. Biophys. Acta 1818 (2) (2012) 154–161.
[28] J.R. Lakowicz, Principles of Fluorescence Spectroscopy, Springer, New York, 2006.
[29] M.R. Eftink, C.A. Ghiron, Exposure of tryptophanyl residues in proteins. Quantitative determination by fluorescence quenching studies, Biochemistry 15 (3) (1976) 672–680.
[30] M.R. Eftink, T.J. Selva, Z. Wasylewski, Studies of the efficiency and mechanism of fluorescence quenching reactions using acrylamide and succinimide as quenchers, Photochem. Photobiol. 46 (1) (1987) 23–30.
[31] J.R. Lakowicz, B. Zelent, I. Gryczynski, J. Kuba, M.L. Johnson, Distance-dependent fluorescence quenching of tryptophan by acrylamide, Photochem. Photobiol. 60 (3) (1994) 205–214.
[32] M.R. Eftink, C.A. Ghiron, Fluorescence quenching studies with proteins, Anal. Biochem. 114 (2) (1981) 199–227.
[33] J.H. Kleinschmidt, L.K. Tamm, Time-resolved distance determination by tryptophan fluorescence quenching: probing intermediates in membrane protein folding, Biochemistry 38 (1999) 4996–5005.
[34] N.A. Rodionova, S.A. Tatulian, T. Surrey, F. Jaehnig, L.K. Tamm, Characterization of two membrane-bound forms of OmpA, Biochemistry 34 (6) (1995) 1921–1929.
[35] W.C. Wimley, M.E. Selsted, S.H. White, Interactions between human defensins and lipid bilayers: evidence for formation of multimeric pores, Protein Sci. 3 (9) (1994) 1362–1373.
[36] Ø. Strømland, S. Handegård Ø, M.L. Govasli, H. Wen, S. Furse, Ø. Halskau, Spectroscopic and AFM characterization of polypeptide-surface interactions: Controls and lipid quantitative analyses, Data Brief 12 (2017) 113–122.
[37] M. Biomedicals, TRITON® X-100, 02300221, 2016.
[38] A.S. Ladokhin, W.C. Wimley, S.H. White, Leakage of membrane vesicle contents: determination of mechanism using fluorescence requenching, Biophys. J. 69 (1995) 1964–1971.
[39] B.J.P. Berne, Dynamic Light Scattering: With Applications to Chemistry, Biology, and Physics, Dover, Mineola, New York, 2006.
[40] J.E. Kim, G. Arjara, J.H. Richards, H.B. Gray, J.R. Winkler, Probing folded and unfolded states of outer membrane protein A with steady-state and time-resolved tryptophan fluorescence, J. Phys. Chem. B 110 (35) (2006) 17656–17662.
[41] A.B. Ghisaidoobe, S.J. Chung, Intrinsic tryptophan fluorescence in the detection and analysis of proteins: a focus on Förster resonance energy transfer techniques, Int. J. Mol. Sci. 15 (2014) 22518–22538.
[42] A.G. Szabo, D.M. Rayner, Fluorescence decay of tryptophan conformers in aqueous solution, J. Am. Chem. Soc. 102 (2) (1980) 554–563.
[43] K. Kawahara, C. Tanford, Viscosity and density of aqueous solutions of urea and guanidine hydrochloride, J. Biol. Chem. 241 (13) (1966) 3228–3232.
[44] M.R. Eftink, C.A. Ghiron, Exposure of tryptophanyl residues and protein dynamics, Biochemistry 16 (25) (1977) 5546–5551.
[45] W.D. McCubbin, C.M. Kay, Acrylamide fluorescence quenching studies on skeletal and cardiac troponins, FEBS Lett. 122 (1980) 72–76.
[46] J. Qu, C. Mayer, S. Behrens, O. Holst, J.H. Kleinschmidt, The trimeric periplasmic chaperone Skp of *Escherichia coli* forms 1:1 complexes with outer membrane proteins via hydrophobic and electrostatic interactions, J. Mol. Biol. 374 (2007) 91–105.
[47] E.J. Danoff, K.G. Fleming, The soluble, periplasmic domain of OmpA folds as an independent unit and displays chaperone activity by reducing the self-association propensity of the unfolded OmpA transmembrane β-barrel, Biophys. Chem. 159 (1) (2011) 194–204.
[48] L.K. Tamm, H. Hong, B. Liang, Folding and assembly of β-barrel membrane proteins, Biochim. Biophys. Acta 1666 (1-2) (2004) 250–263.
[49] J.D. Bryngelson, José.N. Onuchic, N.D. Socci, P.G. Wolynes, Funnels, pathways, and the energy landscape of protein folding: a synthesis, Proteins 21 (3) (1995) 167–195.
[50] N.K. Burgess, T.P. Dao, A.M. Stanley, K.G. Fleming, Beta-barrel proteins that reside in the *Escherichia coli* outer membrane in vivo demonstrate varied folding behavior in vitro, J. Biol. Chem. 283 (2008) 26748–26758.
[51] Z.V. Leonenko, E. Finot, H. Ma, T.E.S. Dahms, D.T. Cramb, Investigation of temperature-induced phase transitions in DOPC and DPPC phospholipid bilayers using temperature-controlled scanning force microscopy, Biophys. J. 86 (6) (2004) 3783–3793.
[52] E.J. Danoff, K.G. Fleming, Novel kinetic intermediates populated along the folding pathway of the transmembrane β-barrel OmpA, Biochemistry 56 (1) (2017) 47–60.
[53] M.A. Bahri, B.J. Heyne, P. Hans, A.E. Seret, A.A. Mouithys-Mickalad, M.D. Hoebeke, Quantification of lipid bilayer effective microviscosity and fluidity effect induced by propofol, Biophys. Chem. 114 (1) (2005) 53–61.
[54] K.M. Sanchez, G. Kang, B. Wu, J.E. Kim, Tryptophan-lipid interactions in membrane protein folding probed by ultraviolet resonance Raman and fluorescence spectroscopy, Biophys. J. 100 (9) (2011) 2121–2130.
[55] S. Ohnishi, K. Kameyama, *Escherichia coli* OmpA retains a folded structure in the presence of sodium dodecyl sulfate due to a high kinetic barrier to unfolding, Biochim. Biophys. Acta. 1515 (2) (2001) 159–166.
[56] J.H. Kleinschmidt, L.K. Tamm, Secondary and tertiary structure formation of the beta-barrel membrane protein OmpA is synchronized and depends on membrane thickness, J. Mol. Biol. 324 (2002) 319–330.
[57] G. Kang, I. López-Peña, S. Bhakta, J.E. Kim, Probing Membrane Protein Structure and Dynamics by Fluorescence Spectroscopy, John Wiley & Sons Ltd, 2013.
[58] C.G. Malmberg, A.A. Maryott, Dielectric constant of water from 0 degree to 1000 degree C, J. Res. Natl. Bur. Stand. 56 (1956) 1–8.
[59] A. Raudino, D. Mauzerall, Dielectric properties of the polar head group region of zwitterionic lipid bilayers, Biophys. J. 50 (3) (1986) 441–449.
[60] F. Bellemare, M. DeMendoncaFragata, Polarity studies on the head group of single-layered phosphatidylcholine – tocopherol vesicles, J. Colloid Interface Sci. 77 (1980) 243–251.
[61] R. Fettiplace, D.M. Andrews, D.A. Haydon, The thickness, composition and structure of some lipid bilayers and natural membranes, J. Membr. Biol. 5 (3) (1971) 277–296.
[62] C.C. Wang, L.J. Bruner, Evidence for a discrete charge effect within lipid bilayer membranes, Biophys. J. 24 (3) (1978) 749–764.
[63] CRC, Handbook of Chemistry and Physics, 43 ed., The Chemical Rubber Publishing Company, Cleveland Ohio, 1961.
[64] H.M. Badawi, M.A.A. Al-Khaldi, S.S.A. Al-Abbad, Z.H.A. Al-Sunaidi, Rotational barriers in monomeric CH2CX–COOH and CH2CX–CONH2 (X is H or CH3) and vibrational analysis of methacrylic acid and methacrylamide, Spectrochim. Acta, Part A 68 (3) (2007) 432–442.
[65] B.A. Lewis, D.M. Engelman, Lipid bilayer thickness varies linearly with acyl chain length in fluid phosphatidylcholine vesicles, J. Mol. Biol. 166 (2) (1983) 211–217.
[66] G.A. Caputo, E. London, Using a novel dual fluorescence quenching assay for measurement of tryptophan depth within lipid bilayers to determine hydrophobic α-helix locations within membranes, Biochemistry 42 (11) (2003) 3265–3274.

[67] F. Moro, F.M. Goñi, M.A. Urbaneja, Fluorescence quenching at interfaces and the permeation of acrylamide and iodide across phospholipid bilayers, FEBS Lett. 330 (1993) 129–132.

[68] K.M. Sanchez, T.J. Neary, J.E. Kim, Ultraviolet resonance Raman spectroscopy of folded and unfolded states of an integral membrane protein, J. Phys. Chem. B 112 (31) (2008) 9507–9511.

[69] P. Kaszycki, Z. Wasylewski, Fluorescence-quenching-resolved spectra of melittin in lipid bilayers, Biochim. Biophys. Acta 1040 (3) (1990) 337–345.